Monthly Notices
of the
ROYAL ASTRONOMICAL SOCIETY

MNRAS **473,** 328–335 (2018)
Advance Access publication 2017 September 22

doi:10.1093/mnras/stx2419

Massive black holes from dissipative dark matter

Guido D'Amico,[1★†] Paolo Panci,[1★†] Alessandro Lupi,[2] Stefano Bovino[3] and Joe Silk[2,4,5]

[1]*CERN Theoretical Physics Department, Case C01600, CH-1211 Genève, Switzerland*
[2]*Institut d'Astrophysique de Paris, UMR 7095 CNRS, Université Pierre et Marie Curie, 98 bis Boulevard Arago, F-75014 Paris, France*
[3]*Hamburger Sternwarte, Universität Hamburg, Gojenbergsweg 112, D-21029 Hamburg, Germany*
[4]*The Johns Hopkins University, Department of Physics and Astronomy, 3400 N. Charles Street, Baltimore, MD 21218, USA*
[5]*Beecroft Institute of Particle Astrophysics and Cosmology, Department of Physics, University of Oxford, 1 Keble Road, Oxford OX1 3RH, UK*

Accepted 2017 September 15. Received 2017 September 15; in original form 2017 July 22

ABSTRACT

We show that a subdominant component of dissipative dark matter resembling the Standard Model can form many intermediate-mass black hole seeds during the first structure formation epoch. We also observe that, in the presence of this matter sector, the black holes will grow at a much faster rate with respect to the ordinary case. These facts can explain the observed abundance of supermassive black holes feeding high-redshift quasars. The scenario will have interesting observational consequences for dark substructures and gravitational wave production.

Key words: black hole physics – galaxies: formation.

1 INTRODUCTION

Galaxy formation is a complex process. Despite continuing efforts incorporating higher resolution numerical simulations with more and more sophisticated subgrid stellar physics, it has hitherto proven impossible to satisfy observational constraints simultaneously at both dwarf and massive galaxy scales. Introduction of feedback from massive black holes has helped alleviate the problem of excessive production of massive galaxies (Genel et al. 2014), but nearby dwarf galaxies provide a well studied and more challenging environment. Supernova feedback seems incapable of resolving their paucity (Bland-Hawthorn, Sutherland & Webster 2015), the too-big-to-fail problem (Garrison-Kimmel et al. 2013) and the 'missing' baryon fraction issue (Bregman et al. 2015).

This failure has motivated many attempts at modifying the nature of dark matter (DM), for example into warm (Dodelson & Widrow 1994; Dolgov & Hansen 2002; Bose et al. 2017), fuzzy (Hu, Barkana & Gruzinov 2000; Marsh & Silk 2014) and strongly self-interacting (Spergel & Steinhardt 2000; Elbert et al. 2015) variants. All of these attempts seem to create as many problems as they try to resolve (Schneider et al. 2016).

Here, we take a different tack via the mirror DM (Berezhiani 2005; Foot 2004; Blinnikov & Khlopov 1983; Khlopov et al. 1991). We demonstrate that a subdominant component of dissipative DM, containing dark baryons and dark photons identical to ordinary sector particles, naturally produces intermediate-mass black holes (IMBHs), in the mass range 10^4–10^5 $M_\odot$, at the epoch of first structure formation. This behaviour derives from the suppression of mirror molecular hydrogen, due to a much lower fraction of free mirror electrons, which act as catalysers.

By accretion, a few of these BHs can transform into the supermassive black holes (SMBHs) observed at $z \sim 7$ (see Valiante et al. 2017, and references therein), whose existence is still an unexplained issue in astrophysics. This can happen because we have massive seeds and they can accrete two non-interacting dissipative matter sectors (ordinary and mirror).

The paper is organized as follows. In Section 2, we describe our DM model, whose thermal history we study in Section 3. Section 4 is devoted to the description of the structure formation in the mirror sector and the estimate of the IMBH number density. We discuss the accretion of the BH seeds in Section 5, and summarize our results in Section 6.

2 MIRROR WORLD

We assume the existence of a parallel sector of mirror particles, which is completely identical, in terms of particle physics properties, to the Standard Model (SM) particle sector. Mirror particles interact with the SM only via gravitational interactions and all the portals (e.g. photon and Higgs portals) are chosen to be very small. We further assume the existence of a cold DM component, which does not interact appreciably with the baryons (ordinary and mirror).

We leave the particle physics details to future work. For the purpose of this article, it will suffice to note that, in the simplest scenario, the whole theory is invariant with respect to an unbroken

★ E-mail: damico.guido@gmail.com (GD); paolo.panci@cern.ch (PP)
† These two authors contributed equally.

discrete mirror parity that exchanges the fields in the two sectors, although there needs to be a breaking in the very early Universe to allow different initial conditions in the two sectors Berezhiani, Comelli & Villante (2001b). The DM component can simply be an axion, i.e. the Goldstone of an anomalous, spontaneously broken $U(1)_{\rm PQ}$ Peccei–Quinn (PQ) symmetry, with the $U(1)_{\rm PQ}$ charges carried by both the ordinary and mirror Higgses (for an example, see Berezhiani, Gianfagna & Giannotti 2001a). In summary, from a cosmological point of view, we have the following:

(i) *A duplicate of the SM matter*. The relativistic degrees of freedom of this sector are mirror photons and neutrinos, contributing an energy density $\Omega'_{\rm r}$. The non-relativistic degrees of freedom are mirror baryons with energy density $\Omega'_{\rm b}$. Here and in the following, the symbol ($'$) denotes the physical quantities of the mirror world.

(ii) *A cold dark matter* (*CDM*) *candidate*. Its energy density is denoted $\Omega_{\rm c}$, such that the total matter energy fraction is $\Omega_{\rm m} = \Omega_{\rm c} + \Omega_{\rm b} + \Omega'_{\rm b}$.

All the differences between the two sectors can be described in terms of two macroscopic parameters, which are the only free parameters of the model:

$$x = T'_\gamma/T_\gamma, \qquad \beta = \Omega'_{\rm b}/\Omega_{\rm b}, \tag{1}$$

T_γ being the photon temperature. For simplicity, the results showed in the next sections are derived by taking $\beta = 1$, i.e. $\Omega'_{\rm b} = \Omega_{\rm b}$.

In order to avoid the cosmic microwave background (CMB) and big bang nucleosynthesis (BBN) bounds on dark radiation, one needs the condition $x \lesssim 0.3$ (Berezhiani et al. 2001b; Foot & Vagnozzi 2015). If this is the case, we will see in the next section that mirror matter behaves like CDM at the time of CMB last scattering. (Mirror baryons are bounded in neutral mirror hydrogen atoms.)

3 A BRIEF THERMAL HISTORY OF THE MIRROR UNIVERSE

As discussed, in our setup the Friedmann equation reads

$$H(z) = H_0 \Big[\Omega_{\rm r}(1+x^4)(1+z)^4 + (\Omega_{\rm b}(1+\beta)+\Omega_{\rm c})(1+z)^3 + \Omega_\Lambda\Big]^{1/2} \tag{2}$$

where H_0 is today's Hubble constant.

An important stage for structure formation is the matter–radiation equality epoch, which occurs at the redshift

$$1 + z_{\rm eq} = \frac{\Omega_{\rm m}}{\Omega_{\rm r}^{\rm tot}} = \frac{\Omega_{\rm b}(1+\beta)+\Omega_{\rm c}}{\Omega_{\rm r}(1+x^4)} = \frac{\rho_{\rm c}^0}{T_{\gamma,0}^4}\,\frac{\Omega_{\rm m}}{\pi^2/30\, g_*(T_{\gamma,0})\,(1+x^4)}\,, \tag{3}$$

where g_* is the number of relativistic degrees of freedom and $T_{\gamma,0}$ is the CMB temperature today. Using the best-fitting Planck parameters (Ade et al. 2016), one gets $1 + z_{\rm eq} \simeq 3396/(1+x^4)$. Since $x \ll 1$, the matter–radiation equality is untouched in the presence of a colder mirror sector.

The evolution of the free electron number fraction $X_{\rm e}$ and gas temperature $T_{\rm g}$ as a function of the redshift z for the ordinary and mirror sectors are ruled by the following coupled differential equations (Giesen et al. 2012):

$$\frac{{\rm d}X_{\rm e}}{{\rm d}z} = \frac{\mathcal{P}_2}{(1+z)H(z)}\Big(\alpha_{\rm H}(T_{\rm g})n_{\rm H}X_{\rm e}^2 - \beta_{\rm H}(T_{\rm g}){\rm e}^{-E_\alpha/T_{\rm g}}(1-X_{\rm e})\Big), \tag{4}$$

$$\frac{{\rm d}T_{\rm g}}{{\rm d}z} = \frac{1}{1+z}\left[2T_{\rm g} - \gamma_{\rm C}\left(T_\gamma(z) - T_{\rm g}\right)\right], \tag{5}$$

where E_α is the Ly α energy, $\beta_{\rm H}$ is the effective photoionization rate from $n = 2$ (per atom in the 2s state) and $\alpha_{\rm H}$ is the case-B recombination coefficient. We have defined the dimensionless coefficient

$$\gamma_{\rm C} \equiv \frac{8\sigma_{\rm T}a_{\rm r}T_\gamma^4}{3Hm_{\rm e}c}\,\frac{X_{\rm e}}{1+X_{\rm He}+X_{\rm e}}\,, \tag{6}$$

(and analogous for the mirror sector) with $\sigma_{\rm T}$ is the Thomson cross-section, $a_{\rm r}$ is the radiation constant, $m_{\rm e}$ is the electron mass and $X_{\rm He}$ is the number fraction of helium. The coefficient $\mathcal{P}_2$ represents the probability for an electron in the $n = 2$ state to get to the ground state before being ionized, given by (Giesen et al. 2012)

$$\mathcal{P}_2 = \frac{1 + K_{\rm H}\Lambda_{\rm H}n_{\rm H}(1-X_{\rm e})}{1 + K_{\rm H}(\Lambda_{\rm H}+\beta_{\rm H})n_{\rm H}(1-X_{\rm e})}\,, \tag{7}$$

(and analogous expression for the mirror sector) where $\Lambda_{\rm H} = 8.22458\,{\rm s}^{-1}$ is the decay rate of the 2s level, and $K_{\rm H} = \lambda_{{\rm Ly}\alpha}^3/(8\pi H(z))$ accounts for the cosmological redshifting of the Ly α photons.

For the ordinary sector, the boundary conditions are $X_{\rm e}(z_M) = 1$ and $T_{\rm g}(z_M) = T_{\gamma,0}(1+z_M)$.[1] For the mirror sector, the equations take the same form, with the substitutions $X_{\rm e} \to X'_{\rm e}$, $T_{\rm g} \to T'_{\rm g}$, $n_{\rm H} \to n_{\rm H'}$, $\gamma_{\rm C} \to \gamma'_{\rm C}$, $T_\gamma(z) \to x\,T_\gamma(z)$. The boundary conditions in the mirror sector are $X'_{\rm e}(z_M/x) = 1$ and $T'_{\rm g}(z_M/x) = T_{\gamma,0}(1+z_M/x)$.

From equation (6) in the mirror sector, we notice that the Compton rate is a factor of x^4 smaller than that in the ordinary sector. As a consequence, the recombination in the speculative sector is much faster. We solve numerically equations (5), showing the results in Fig. 1. The left-hand panel shows the electron fraction $X_{\rm e}$ for the ordinary and mirror sectors as a function of redshift. For the mirror sector, we show the results for three benchmark values of x: $x = 0.3$ (blue dot–dashed line), $x = 0.1$ (magenta dot–dashed line) and $x = 0.01$ (red dot–dashed line).

At the time of the ordinary recombination ($z \simeq 1100$) the mirror hydrogen is fully recombined. Indeed, the residual mirror ionization fraction $X'_{\rm e}$ at $z = 1100$ is always less than 10^{-5} for the three benchmark models we consider. As a consequence, mirror hydrogen behaves like CDM with respect to the ordinary plasma evolution before the CMB last scattering. Hence, by $z \simeq 1100$, the total amount of CDM is exactly the one measured by the *Planck* satellite: i.e. $\Omega_{\rm DM} = \Omega_{\rm m} - \Omega_{\rm b} = \Omega'_{\rm b} + \Omega_{\rm c}$. The right-hand panel of Fig. 1 shows instead the evolution of the gas temperatures $T_{\rm g}$, $T'_{\rm g}$ as a function of redshift. Since the Compton heating process is not efficient in keeping the mirror baryons and mirror photons in thermal equilibrium, the temperature of the mirror gas at redshifts relevant for the structure formation is much smaller than the ordinary one (not simply by a factor of x).

[1] Here $z_M = 2500$. We have checked that for $z > z_M$ the solutions are stable.

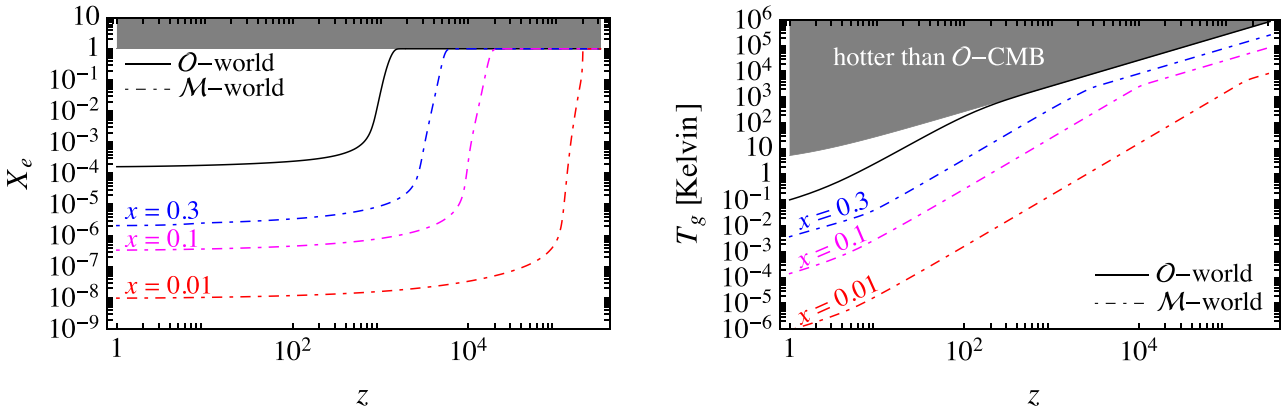

Figure 1. Left-hand panel:free electron number abundance X_e as a function of redshift z for the ordinary (black solid), and mirror sector for different values of the x parameter (dot–dashed lines). Right-hand panel: background gas temperature T_g as a function of redshift z.

4 STRUCTURE FORMATION

4.1 Qualitative picture

The different chemical initial conditions of the ordinary and mirror gas are crucial for understanding the differences in the formation of the first structures in the two sectors.

Let us follow a spherical overdensity of mirror baryons. While $\delta \equiv \rho/\rho \ll 1$, it will expand with the rest of the universe, but lagging behind as $\delta\rho \sim a^{-2}$. At some point, when $\delta \sim 4.55$, the overdensity turns around and starts to collapse (Mo, van den Bosch & White 2010). If the matter interacts only gravitationally (as the CDM component), the final result of the collapse will be a halo of particles supported by velocity dispersion, corresponding to an effective virial temperature $T_{\rm vir} = \mu m_{\rm p} G_N M/(5 k_{\rm B} R)$, where μ is the mean molecular weight, $m_{\rm p}$ the proton mass, and M, R the mass and radius of the overdensity, respectively. However, unlike CDM, the mirror gas does not undergo shell-crossing, being instead heated by shocks. The end result of the collapse of the gas is approximately a mirror cloud heated to a temperature $\sim(\gamma - 1)T_{\rm vir}$, where $\gamma \simeq 5/3$ is the adiabatic index, at the virial density $\rho_{\rm vir} \simeq 178\, \rho_{\rm cr}\Omega_{\rm b}'(1+z)^3$ (Mo et al. 2010).

At this point, the chemistry of the gas needs to be considered. In particular, we have to ask whether the mirror cloud can cool, losing pressure support and contracting further, or it will remain as a hot dilute halo (resembling a CDM component). At low temperatures, in the absence of heavy elements, there is not enough energy to excite mirror atomic transitions. Therefore, as in the ordinary sector, the main cooling mechanism for a hydrogen–helium gas is through H_2, which at low densities is produced mainly through the reactions $H + e^- \rightarrow H^- + \gamma$, $H^- + H \rightarrow H_2 + e^-$, in which free electrons act as catalysers.

Since molecular cooling can bring the temperature down to $T_{\rm g} \sim 200$ K, ordinary baryons are able to form small structures. However, in the mirror sector the initial abundance of free electrons, as shown in the left-hand panel of Fig. 1, is very suppressed, and therefore the production of mirror molecular hydrogen is slower. This allows some mirror clouds to not undergo catastrophic cooling, as we will show.

First of all, it is clear that mirror clouds with very high virial temperatures, $T_{\rm vir} \gtrsim 10^4$ K, will behave essentially as ordinary clouds, as the mirror hydrogen quickly undergoes full ionization, independently of the initial conditions. The same fate happens to massive clouds, which are adiabatically heated to high temperatures at the beginning of their evolution. On the other hand, at very low virial temperatures, $T_{\rm vir} \lesssim 1000$ K, a mirror cloud is a dilute cloud of neutral atomic hydrogen, which does not cool efficiently (at least in the absence of metals) and just behaves as cold DM, as shown in Section 4.3. We thus expect a range of masses in between these two extrema in which the behaviour of mirror clouds can be different from ordinary baryons.

4.2 Semi-analytical model

We can try to understand more in detail the dynamics of a mirror cloud by considering the evolution of averaged temperature, total number density and species abundances, as done, for instance, in Omukai (2000, 2001). Of course, this is only a first approximation, but it is useful to check the existence of haloes in which very massive BHs may be formed by direct collapse.

The chemistry evolution of the cloud is solved using the KROME package Grassi et al. (2014). For the details about the model, we refer to the built-in one-zone collapse released with the package. We follow the abundance of nine mirror species (H, H^-, p, e, H_2, H_2^+, He, He^+, He^{++}), tracking 21 reactions. For the ordinary sector we use $\mu = 1.22$, corresponding to a gas of hydrogen and helium in their standard BBN abundances. For the mirror sector, we study two models, $x = 0.1$ and 0.01, for which Berezhiani et al. (2001b) showed that the mirror helium abundance is negligible; therefore, we have $\mu' = 1$. The thermodynamic evolution is given by the equation

$$\frac{\dot{T}_{\rm g}}{T_{\rm g}} - (\gamma - 1)\frac{\dot{n}_{\rm g}}{n_{\rm g}} = \frac{(\gamma - 1)}{k_{\rm B} T_{\rm g} n_{\rm g}}(\mathcal{H} - \mathcal{C})\,, \tag{8}$$

where $\mathcal{C}$ and $\mathcal{H}$ are the cooling and heating rates per unit volume, respectively. The inverse of the right-hand side of equation (8) is defined as (minus) the cooling time-scale $t_{\rm c}$. The density evolution is approximated by a free-fall or isobaric evolution, depending on the shorter time-scale between the sound-crossing time $t_{\rm s}$ and the free-fall time $t_{\rm ff}$.[2] If $t_{\rm s} > t_{\rm ff}$, we take the number density evolution to be $\dot{n}_{\rm g} = n_{\rm g}/t_{\rm ff}$ Omukai (2000); if instead $t_{\rm s} < t_{\rm ff}$, the number density is inversely proportional to the temperature, $n_{\rm g} \propto T_{\rm g}^{-1}$.

Our results are shown in Fig. 2, which illustrates the evolution of several physical quantities as a function of the gas density $n_{\rm g}$

[2] The sound-crossing time is $t_{\rm s} = R/c_{\rm s}$, where R is the radius of the cloud and c_s is the sound speed. The free-fall time is $t_{\rm ff} = (3\pi/(32\, G\rho_{\rm tot}))^{1/2}$, $\rho_{\rm tot}$ being the total mass density.

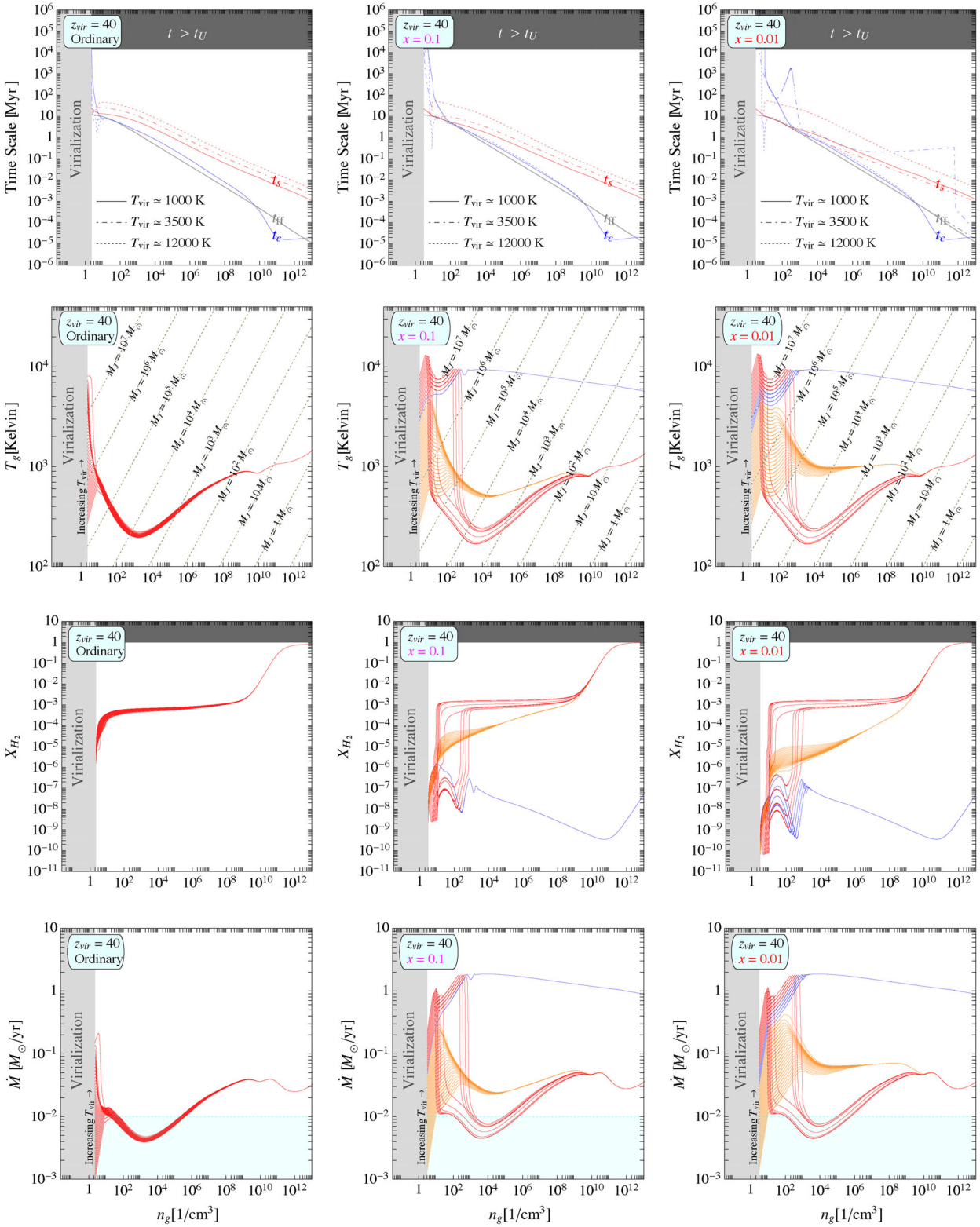

Figure 2. Evolution of several physical quantities as a function of the gas number density n_g at $z_{vir} = 40$. The panels in the first column describe the properties of the ordinary sector, while the second and third columns refer to the mirror sectors with $x = 0.1$ and 0.01, respectively. In all plots, the light grey area on the left-hand side denotes the region of the parameter space where the gas is not yet virialized. First row: evolution of the free-fall t_{ff} (grey lines), sound-crossing t_s (red lines) and cooling t_c (blue lines) time-scales for three virial temperatures [$T_{vir} = 1000$ K (solid lines), $T_{vir} = 3500$ K (dot–dashed lines] and $T_{vir} = 12000$ K (dotted lines)). Second row: evolution of the gas temperature T_g. Three scenarios are possible: efficient gas cooling at $\sim$200 K (red lines); quasi-isothermal collapse in the range $\sim 500-900$ K (orange lines, depending on the value of x); quasi-isothermal collapse at $\sim$9000 K (blue lines). Third row: evolution of the number fraction of molecular hydrogen X_{H_2} for the scenarios discussed before. Fourth row: evolution of the mass accretion rate estimated as the Jeans mass to free-fall time $\dot{M} = M_J/t_{ff}$. The cyan region gives a threshold above which a DCBH is possible.

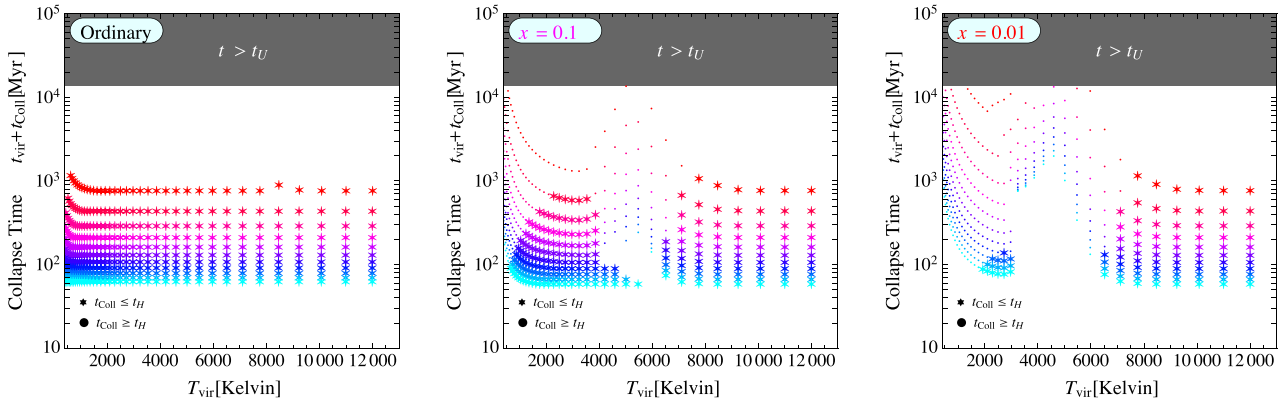

Figure 3. Typical collapse time-scales as a function of the virial temperature T_{vir}. From the left- to the right-hand side, we show the ordinary and the mirror sectors with $x = 0.1$ and 0.01, respectively. For a given T_{vir}, the different points are obtained by assuming several virialization redshifts. From the bottom ($z_{vir} = 60$) to top ($z_{vir} = 10$) the step in redshift is $\Delta z = 5$. The stars satisfy the criterium $t_{Coll} < t_H$ while the dots do not.

at a virialization redshift $z_{vir} = 40$. From the top to bottom, the rows show the evolution of free-fall, sound-crossing and cooling time-scales; gas temperature T_g; the number fraction of molecular hydrogen X_{H_2}; and finally the accretion rate, estimated as $\dot{M} = M_J/t_{ff}$, where M_J is the Jeans mass. From the left- to the right-hand side, we show the ordinary sector, the mirror with $x = 0.1$ and the mirror with $x = 0.01$. From the second to the fourth row, the different curves correspond to different halo virial masses.

Focusing on the phase diagram ($T_g - n_g$), we can see that all the haloes of the ordinary sector, after an initial phase of adiabatic contraction (in some cases followed by a short isobaric evolution) produce enough molecular hydrogen to quickly cool down to ∼200 K (red lines), according to the results reported in Omukai (2000, 2001). The mirror sectors, instead, shows markedly different behaviour for moderate virial temperatures. First, as shown by the red curves, the more massive haloes that manage to attain a temperature above the Ly α line will ionize the mirror neutral hydrogen, thus behaving as ordinary haloes. However, at lower virial temperatures, the orange curves show that the evolution settles down to a quasi-isothermal collapse at a temperature in the range ∼500–900 K (depending on the value of x), at least until the density reaches 10^{10} cm^{-3}, when three-body reactions become important. As apparent from the evolution of the time-scales and of the H_2 abundance, this behaviour is due to a balance between the cooling induced by trace amounts of molecular hydrogen and the compressional heating. We also observe a third qualitative behaviour in a narrow range of virial masses, illustrated by the blue curves. These haloes follow a trajectory, which brings them close to the Ly α line, and they start to produce molecular hydrogen. However, before cooling occurs, the density reaches a critical value for which the cooling function changes behaviour in n_g Le Bourlot, Pineau des Forêts & Flower (1999). After that, there is a collapse in which the temperature decreases very slowly, with negligible amounts of H_2. The end result of this scenario looks somewhat similar to the case in which molecular hydrogen is destroyed by Lyman–Werner photons Bromm & Loeb (2003), but in our case the time evolution of the haloes is very slow (∼Gyr). Therefore, as we discuss below, these haloes cannot collapse fast enough before undergoing merger events.

At this point, we would like to discuss the endpoint of the collapse of ordinary and mirror haloes, whether we produce Population III (POPIII) stars or direct collapse black holes (DCBHS). We rely on the results of Ferrara et al. (2014) and Latif & Ferrara (2016), which give a threshold $\dot{M} \sim 10^{-2}\,M_\odot\,yr^{-1}$ above which the result of the halo collapse is a DCBH. This is shown as the cyan region in the last row of Fig. 2. If we choose to evaluate $\dot{M}$ when the halo reaches a minimum temperature, which presumably means it fragments into Jeans-supported structures, we find that the ordinary sector can only form POPIII stars, while the mirror sector is able to form DCBHS in the cases represented by the orange and blue curves (which, however, evolve too slowly). From the dashed black lines depicted in the second row of Fig. 2 we estimate the mass of such BHs, *at their formation time*, as $(10^4-10^5)\,M_\odot$, the Jeans mass at (presumed) fragmentation (for the orange curves). The number of BHs, we expect to form can be as low as a few and as high as $(\Omega_b'/\Omega_c)\,M_{vir}/M_{J,min}$, where M_{vir} is the virial mass of the original halo and $M_{J,\,min}$ is the Jeans mass at the temperature minimum. For illustration, in the mirror sector with $x = 0.1$, the maximum number of DCBHs with a mass $\simeq 10^4\,M_\odot$, in a single halo, is in the range 100–500 at $z_{vir} = 40$.

4.3 Time of collapse

Before concluding that each halo produces BHs, we need to check that the single-halo evolution discussed above is a reasonable approximation. In particular, we have neglected the fact that structures in a ΛCDM universe form by continuous merging of smaller objects into larger haloes. Therefore, to be consistent, we have to require that the collapse time t_{Coll} of any halo, defined as the time when the density grows superexponentially, is shorter that a typical 'merger' time-scale, which we take as the Hubble time at the virialization epoch t_H. We show this in Fig. 3. From the left- to the right-hand side, we have the ordinary sector, mirror with $x = 0.1$ and mirror with $x = 0.01$. In each plot, we show the estimated age of the universe when we consider the halo collapsed (and a BH or a star formed), as a function of the virial temperature, for different virialization redshifts (at fixed T_{vir}, the redshift increases from the top to bottom). The grey region represents times larger than the age of the Universe today. The stars denote the haloes that satisfy our criterion that $t_{Coll} < t_H$, while the dots denote the ones that do not.

The evolution of the ordinary sector is always very fast, and we conclude that each halo we consider ends up producing POPIII stars. The evolution in both mirror sectors is instead very different. There are two different ranges in virial temperatures, which we can describe within the single-halo approximation, which correspond to all of the red curves (higher T_{vir}), which end up forming mirror POPIII

Table 1. Number density of candidate haloes, in Gpc^{-3}. For each virialization redshift we show the number density of haloes able to produce DCBHs seed or POPIII star forming sites, as well as the minimum and maximum virial masses, which are the extremes of integration of the Press–Schechter mass function (inferred from Fig. 3). From the left- to the right-hand side, we show results for the ordinary and mirror sectors with $x = 0.1$ and 0.01.

	Ordinary			$x = 0.1$			$x = 0.01$		
	$z_{\rm vir} = 50$	$z_{\rm vir} = 40$	$z_{\rm vir} = 30$	$z_{\rm vir} = 50$	$z_{\rm vir} = 40$	$z_{\rm vir} = 30$	$z_{\rm vir} = 50$	$z_{\rm vir} = 40$	$z_{\rm vir} = 30$
DCBH seeds	0	0	0	403	1.8×10^5	2.7×10^7	0.01	0	0
$M_{\rm vir}^{\rm min}$ ($\mathrm{M}_\odot$)	/	/	/	3.4×10^5	6.2×10^5	1.4×10^6	1.7×10^6	/	/
$M_{\rm vir}^{\rm max}$ ($\mathrm{M}_\odot$)	/	/	/	4.7×10^6	5.0×10^6	7.7×10^6	2.4×10^6	/	/
Star sites	1.1×10^5	3.6×10^7	4.3×10^9	1.2×10^{-8}	0.01	505	1.2×10^{-8}	1.4×10^{-2}	258
$M_{\rm vir}^{\rm min}$ ($\mathrm{M}_\odot$)	9.0×10^4	1.2×10^5	1.9×10^5	8.0×10^6	1.1×10^7	1.9×10^7	8.0×10^6	1.3×10^7	1.9×10^7
$M_{\rm vir}^{\rm max}$ ($\mathrm{M}_\odot$)	∞	∞	∞	∞	∞	∞	∞	∞	∞

stars, and some of the orange curves (lower $T_{\rm vir}$) in Fig. 2, which end up forming IMBH seeds. As anticipated, all the blue curves in Fig. 2 evolve so slowly we cannot really trust our conclusions. We can say the same about the small haloes with low $T_{\rm vir}$ (dots on the left in the mirror panels of Fig. 3). These will evolve very slowly, thus resembling a CDM component before undergoing mergers with other haloes.

4.4 Number of candidate haloes

Finally, we would like to estimate the number of BH seeds produced by the mirror sector. We can say that each halo that undergoes quasi-isothermal collapse at $T_{\rm g} \simeq 500-900$ K (orange lines in the second panel of Fig. 2) could hosts at least one, at most $(\Omega_{\rm b}'/\Omega_{\rm c})\, M_{\rm vir}/M_{\rm J}$ BHs. An approximate answer to our question is the estimate of the number of such haloes, which we will do using the Press–Schechter mass function. In detail, we integrate the mass function over the ranges of halo virial masses able to produce DCBHs or stars, as identified in Fig. 3. Our results, in number of haloes per comoving Gpc^3, are shown in Table 1, for three representative redshifts of virialization ($z_{\rm vir} = 30, 40, 50$).

As one can see the amount of haloes containing stars in the mirror sector is much smaller with respect to the ordinary sector, especially at high redshift. We then expect that the mirror sector is, in general, less contaminated by metals, which cause halo cooling and fragmentation. This can be understood by noticing that, in the case of the lowest virialization redshift we use ($z_{\rm vir} = 30$), in the ordinary sector there is already one star formation site per halo with a mass above $\simeq 2 \times 10^5\,\mathrm{M}_\odot$ (corresponding to the lowest virial temperature we consider). Indeed, our estimate is of the same order ($\sim 10^9/\mathrm{Gpc}^3$ when the Universe was $t_{\rm vir}(z = 30) + t_{\rm coll} \simeq 200$ Myr old) of the (extrapolated) galaxy number density of the Universe (Conselice et al. 2016; Bouwens et al. 2015; Stark et al. 2013), while in the mirror sector we expect the star formation sites to be in negligible number ($\sim$500). For this reason, we do not fully trust our calculations at a lower redshift, as we expect that at least the ordinary sector is polluted by metals, thus changing the collapse dynamics of both the ordinary and the mirror sector.

The star formation history in the mirror sector is different than in the ordinary sector, and we expect that mirror stars are less abundant and bigger than the ordinary ones, at the same epoch. Furthermore, for the mirror sector with $x = 0.1$, we estimate that there are many DCBH seeds ($\sim 10^7\ \mathrm{Gpc}^{-3}$), more than the mirror star formation sites. From the numbers we get, we estimate that DCBH seeds are about a factor of 10^{-2} less abundant than the sites of star formation in the ordinary sector; in other words, we expect that about one percent of galaxies will host a BH.

As for the sector with $x = 0.01$, we see that it forms very few DCBH seeds, formed only above $z = 40$, and a few mirror stars. Indeed, this sector is very cold and remains mostly dilute during the cosmic evolution.

5 ACCRETION OF BH SEEDS

Our results so far give an interesting indication that many haloes can produce very massive BH seeds, by direct collapse of mirror baryon clouds. The next question is to understand whether we can reach BH masses of up to $10^9 - 10^{10}\,\mathrm{M}_\odot$ by redshift $\sim$7, as observed by Valiante et al. (2017).

After formation, we expect that the seed BH will grow by accretion, of both ordinary and mirror baryons. In first approximation, we assume (Yoo & Miralda-Escudé 2004) that a BH formed at time t_0 with mass M_0 grows continuously to reach a mass at time t

$$M(t) = M_0\, \mathrm{e}^{(t-t_0)/t_{\rm Sal}}\,. \tag{9}$$

Here, $t_{\rm Sal}$ is the Salpeter time (Salpeter 1964)

$$t_{\rm Sal} = \frac{\epsilon M c^2}{(1-\epsilon)L} \simeq 400\,\mathrm{Myr}\frac{\epsilon}{1-\epsilon}\frac{L_{\rm Edd}}{L}\,, \tag{10}$$

where ϵ is the radiative efficiency, L is the BH luminosity and $L_{\rm Edd}$ is the Eddington luminosity. In the presence of an ordinary and a mirror sector, which interact only gravitationally with each other, we expect that the Salpeter time roughly halves, assuming that the accretion happens in both sectors at similar luminosity and efficiency. Therefore, in a universe with both ordinary and mirror matter, even small seed BHs grow very fast, with an e-folding timescale of $\sim$22 Myr if the accretion happens at Eddington luminosity and $\epsilon \simeq 0.1$. Now, focusing on the mirror sector with $x = 0.1$, by $z_{\rm vir} = 30$ we have a large amount of DCBH seeds ($\sim 10^7/\mathrm{Gpc}^3$) with initial masses $M_0 \simeq 10^4\,\mathrm{M}_\odot$ formed when the Universe was $t_{\rm vir}(z = 30) + t_{\rm Coll} \equiv t_0 \simeq 200$ Myr. By substituting these numbers in equation (9), we get that, at the time $t(z = 7) \simeq 800$ Myr when SMBHs with mass bigger than $10^9\,\mathrm{M}_\odot$ are observed (Mortlock et al. 2011), in our framework we are able to saturate such high masses even if the DCBH seeds continuously accrete mass with a high radiative efficiency and luminosity less than Eddington in either sector. As far as we know, ours is the only model[3] that can accelerate the BH growth so quickly. Even significant super-Eddington growth of SMBHs in the ordinary sector requires seed BHs of at least $\sim 100\,\mathrm{M}_\odot$ present at $z \sim 20$ (Pezzulli et al. 2016), and in any case

[3] More generally, this happens in models with dissipative matter which can form dense structures.

observations of the SMBH in quasars point out to accretion at a fraction of the Eddington luminosity (Trakhtenbrot et al. 2017).

Nevertheless, we cannot reliably estimate the final mass reached by redshift ∼7 because the exponential accretion is too simple a scenario. There are indeed two major issues to be addressed:

(i) First, there might be radiative feedback effects that shut off the mass accretion above a limiting mass (Ferrara et al. 2014).

(ii) Then, perhaps more importantly, our seed BHs are born in relatively small haloes, of up to $\sim 10^7\,M_\odot$. As a consequence, we should quantify whether the BH, once it has swallowed most of its host environment, can grow further. This will be possible, because of halo accretion. In fact, using the (extrapolation of the) median mass accretion rate derived in Fakhouri, Ma & Boylan-Kolchin (2010), we can determine the evolution of a typical halo by solving $dM/dz = 25.3(1+1.65z)/(1+z)\left[M/(10^{12}\,M_\odot)\right]^{1.1} H_0^{-1}\,M_\odot\,yr^{-1}$. Focusing again on the mirror with $x = 0.1$, we estimate that the final halo mass at $z = 7$ is $\sim 10^8\,M_\odot$ and $\sim 1.6\times 10^9\,M_\odot$ for initial virial temperatures $T_{vir} = 1200$ and $T_{vir} = 3900$, respectively, corresponding to the limits of the range of BH-producing haloes virialized at $z_{vir} = 30$ (as shown in Fig. 3). The mass in both baryonic components is a fraction $\Omega_b(1+\beta)/\Omega_m$. The accretion history of a single halo has a large variability in its final mass, and the numbers we quote correspond to a median rate. Given that the largest haloes we consider accrete, in the median, a baryonic mass of the order of the few observed SMBHs, we find it likely that these can be produced by our mechanism.

6 CONCLUSIONS AND OUTLOOK

The presence of SMBHs at redshift as high as 7 is still an open issue in astrophysics. Moreover, baryonic feedback by supernovae has difficulty in resolving outstanding problems in dwarf galaxy formation. A new ingredient may be needed that might involve IMBH feedback in dwarfs, but it is far from obvious how such IMBH might form in the early universe.

We provide a DM solution to this problem by appealing to a subdominant dissipative component of the dark sector, which for simplicity we consider to be a mirror copy of the SM, while the rest of the DM sector is assumed to be a standard cold candidate. Concerning the particle physics details, we have in mind a model consisting of a mirror copy of the SM with the same coupling constants and masses, with an axion-like particle shared by both ordinary and mirror sector. The axion can potentially solve the strong-CP problem (Berezhiani et al. 2001a), but we leave the details to future work.

Of course, this is not the only model that can give the phenomenology we discussed. We expect that similar conclusions can be reached by changing couplings and masses (or even the particle content). In particular, models with larger binding energy of the dark hydrogen atom will have a larger atomic line cooling temperature, and the cooling by molecular hydrogen is hindered because the formation rate is less efficient. The cooling due to a dark hydrogen-like atom has been recently analysed in Rosenberg & Fan (2017).

Coming back to our mirror scenario, using a zero-dimensional approach, we showed that, if the mirror CMB temperature is much lower than the ordinary one, the thermodynamics and chemistry of collapsing mirror clouds follow a different path, leading to the production of IMBH seeds by direct collapse. We have estimated the frequency, mass range and growth by accretion of the seeds, finding that they might in fact be helpful to resolve the many issues that perplex astrophysicists. More in detail, we expect that by $z \simeq 7$, in the case $x = 0.1$, the bulk of the population of BHs has masses around $10^7 - 10^8\,M_\odot$, with a tail that extends above $\sim 10^9\,M_\odot$, and power the quasars we observe. The mirror sector IMBHs are sufficiently numerous to be at the centres of the dwarf galaxies, such that their feedback could plausibly resolve many of the dwarf galaxy issues in the standard sector. Of course, detailed numerical simulations need to be performed in order to transform our estimates into more precise values, and analyse cosmological data in terms of our scenario.

In addition to the BHs, we will form mirror stars, more massive and much less abundant than in the ordinary sector, as shown in Table 1. In star-forming sites, we expect that part of the dissipative DM will organize itself in discs, rather than haloes. This has been already pointed out in similar models, for instance, in Fan et al. (2013a), Fan et al. (2013b), Agrawal et al. (2017) and Agrawal & Randall (2017). The mirror substructures can be detected by large-scale structure observations, such as lensing, and by small-scale (galactic) probes, such as stellar dynamics.

Today we have a new window to look at the sky: gravitational waves. We expect to have IMBH mergers, and a few mergers of smaller BHs born from the death of mirror stars, at redshifts all the way up to ∼30. While IMBH mergers belong to the LISA range of frequencies, smaller BHs can be observed by LIGO. It is therefore very interesting to evaluate the expected rate and mass range of these merger events.

ACKNOWLEDGEMENTS

We thank Stephane Charlot, Pratika Dayal, Anna Feltre, Andrea Macciò, Mallory Roberts and Dominik Schleicher for useful discussions. PP, JS and AL acknowledge support by the European Research Council (ERC) under the EU Seventh Framework Programme (FP7/2007-2013)/ERC Advanced Grant 267117 ('DARK') hosted by Université Pierre & Marie Curie - Paris 6. AL aknowledges support by the ERC, Project no. 614199 ('BLACK'). SB acknowledges funding through the DFG priority programme 'The Physics of the Interstellar Medium' (projects BO 4113/1-2). PP is grateful to the Institute d'Astrophysique de Paris where this work was initiated.

REFERENCES

Ade P. A. R. et al., 2016, A&A, 594, A13
Agrawal P., Randall L., 2017, preprint (arXiv:1706.04195)
Agrawal P., Cyr-Racine F.-Y., Randall L., Scholtz J., 2017, J. Cosmol. Astropart. Phys., 1708, 021
Berezhiani Z., 2005, in Shifman M. et al., eds, From fields to strings, 3, p. 2147
Berezhiani Z., Gianfagna L., Giannotti M., 2001a, Phys. Lett., B500, 286
Berezhiani Z., Comelli D., Villante F. L., 2001b, Phys. Lett., B503, 362
Bland-Hawthorn J., Sutherland R., Webster D., 2015, ApJ, 807, 154
Blinnikov S. I., Khlopov M. Y., 1983, Soviet Ast., 27, 371
Bose S. et al., 2017, MNRAS, 464, 4520
Bouwens R. J. et al., 2015, ApJ, 803, 34
Bregman J. N., Alves G. C., Miller M. J., Hodges-Kluck E., 2015, J. Astron. Telescopes. Instrum. Syst., 1, 045003
Bromm V., Loeb A., 2003, ApJ, 596, 34
Conselice C. J., Wilkinson A., Duncan K., Mortlock A., 2016, ApJ, 830, 83
Dodelson S., Widrow L. M., 1994, Phys. Rev. Lett., 72, 17
Dolgov A. D., Hansen S. H., 2002, Astropart. Phys., 16, 339
Elbert O. D., Bullock J. S., Garrison-Kimmel S., Rocha M., Oñorbe J., Peter A. H. G., 2015, MNRAS, 453, 29

Fakhouri O., Ma C.-P., Boylan-Kolchin M., 2010, MNRAS, 406, 2267
Fan J., Katz A., Randall L., Reece M., 2013a, Phys. Dark Univ., 2, 139
Fan J., Katz A., Randall L., Reece M., 2013b, Phys. Rev. Lett., 110, 211302
Ferrara A., Salvadori S., Yue B., Schleicher D., 2014, MNRAS, 443, 2410
Foot R., 2004, Int. J. Mod. Phys., D13, 2161
Foot R., Vagnozzi S., 2015, Phys. Rev., D91, 023512
Garrison-Kimmel S., Rocha M., Boylan-Kolchin M., Bullock J. S., Lally J., 2013, MNRAS, 433, 3539
Genel S. et al., 2014, MNRAS, 445, 175
Giesen G., Lesgourgues J., Audren B., Ali-Haimoud Y., 2012, JCAP, 1212, 008
Grassi T., Bovino S., Schleicher D. R. G., Prieto J., Seifried D., Simoncini E., Gianturco F. A., 2014, MNRAS, 439, 2386
Hu W., Barkana R., Gruzinov A., 2000, Phys. Rev. Lett., 85, 1158
Khlopov M. Y., Beskin G. M., Bochkarev N. G., Pustilnik L. A., Pustilnik S. A., 1991, Soviet Ast., 35, 21
Latif M. A., Ferrara A., 2016, PASA, 33, e051
Le Bourlot J., Pineau des Forêts G., Flower D. R., 1999, MNRAS, 305, 802
Marsh D. J. E., Silk J., 2014, MNRAS, 437, 2652
Mo H., van den Bosch F. C., White S., 2010, Galaxy Formation and Evolution. Cambridge Univ. Press, Cambridge
Mortlock D. J. et al., 2011, Nature, 474, 616
Omukai K., 2000, ApJ, 534, 809
Omukai K., 2001, ApJ, 546, 635
Pezzulli E., Valiante R., Schneider R., 2016, MNRAS, 458, 3047
Rosenberg E., Fan J., 2017
Salpeter E. E., 1964, ApJ, 140, 796
Schneider A., Trujillo-Gomez S., Papastergis E., Reed D. S., Lake G., 2016, MNRAS, 470, 1542
Spergel D. N., Steinhardt P. J., 2000, Phys. Rev. Lett., 84, 3760
Stark D. P., Schenker M. A., Ellis R., Robertson B., McLure R., Dunlop J., 2013, ApJ, 763, 129
Trakhtenbrot B., Volonteri M., Natarajan P., 2017, ApJ, 836, L1
Valiante R., Agarwal B., Habouzit M., Pezzulli E., 2017, Publ. Astron. Soc. Aust., 34, 03125
Yoo J., Miralda-Escudé J., 2004, ApJ, 614, L25

This paper has been typeset from a TEX/LATEX file prepared by the author.